A Study of fringe tracking for high precision space-based interferometers

Carlos E. Padilla, Valeri I. Karlov, Jun Li, Hon M. Chun

Moldyn, Inc., 1033 Massachusetts Ave.
Cambridge, MA 02138

John N. Tsitsiklis

Massachusetts Institute of Technology
77 Massachusetts Ave., Cambridge, MA 02139

Robert D. Reasenberg

Harvard-Smithsonian Astrophysical Observatory
60 Garden Street, Cambridge, MA 02138

ABSTRACT

The purpose of the fringe tracking (FT) algorithms is to maintain lock on the target star after acquisition and to obtain the most accurate estimate possible of the scientific quantity (or quantities) of interest in the presence of dynamic disturbances to the spacecraft/inetrferometer ensemble. This study carries out an analysis of the performance and robustness achievable by four candidate estimation techniques when applied to an ultra-high-precision fringe tracking task (5 micro-arcsecond ultimate accuracy). The first class of fringe trackers studied include the Extended Kalman Filter (EKF). This class is followed by extensions to second and third order nonlinear filters developed by the authors. The higher order filters have expanded regions of convergence. Third, we consider the use of an invariant filter (IF) to estimate the angle between two target stars (using POINTS as a test case). The IF offers the advantage of improved robustness in the dynamical case, being in effect "invariant" to dynamics. Finally Discrete Bayes Algorithms (DBA)) make use of Bayes' decision rule to propagate the a posteriori distribution of the true parameter and take into account the discrete character of the Poisson photon arrival events. Variations of these algorithms, known as multiple hypotheses trackers, offer great promise for dim star tracking. An exploration of filter performance with respect to several parameters is carried out analytically and selected Monte Carlo simulations are carried out both to verify analytical predictions and to study performance.

KEYWORDS

Fringe Tracking, Channeled Spectrum, Spaceborne Interferometry, Nonlinear Estimation, Invariant Filter

1. PROBLEM STATEMENT

The fringe tracking (FT) problem follows the fringe acquisition (FA) problem (see Ref. 1). While the goal of the FA problem is in initially estimating the angle that the interferometer optical axis makes with a target star, the goal of the FT problem is in achieving and maintaining the maximum performance over long observation intervals. Using POINTS (Refs. 2-4) as an example, the ultimate objective of the interferometer mission is to obtain a high accuracy estimate of the angular separation between two target stars. This inter-stellar angle is estimated by processing the measurement data from two starlight interferometers mounted at nearly a right angle, and the data from the full aperture laser metrology system (FAM) monitoring the angle between two interferometers.

The specified accuracy of 5 microarcseconds ($\sim 2.4 \times 10^{-11}$ rad) for the angular separation poses a significant challenge

for the FT task since it is necessary to reduce the remaining uncertainty in the angular parameters at the end of the Fringe Acquistion [~ 10^{-7} - 10^{-8} rad] by 3 to 4 orders of magnitude. The main obstacle to achieving the target accuracy is the disturbance environment of the spacecraft, which significantly affects the tracking performance in the range of 10^{-8} - 10^{-11} rad. In this paper, realistic on-board disturbances (for the current stage of research) will be modelled, such as rate gyro (RG) noise, reaction wheel assemblies' (RWA) jitter, and structural modes due to the flexibility of the instrument. The latest design with Fine Pointing and Isolation System (FPIS) will be incorporated into the FT problem to study how the FPIS alleviates the effects of disturbances on the estimation of both the time-varying angle between the interferometer axis and a target star and the constant inter-stellar angle. The high accuracy specifications for the performance also require accounting for possible parametrical and nonparametrical uncertainties in the measurement model such as uncertainties in the visibility (including its functional dependency on optical frequency) and uncertainties in the spectrum (averaged number of detected photons, stellar magnitude and temperature). There are other important parameters such as CCD cell sensitivities (Quantum Efficiency) that we do not explore in this work.

Four major tracking techniques, used in various combinations, are analyzed and implemented in this paper. The first "class" includes the linearized Extended Kalman Filters (EKF). The second "class" introduces the novel Nonlinear EKF (NEKF) which generalizes the EKF in order to optimally robustify it to nonlinearities in the model. The third "class" brings to bear Invariant Filters (IF) which use the recursive mechanism of the EKF or NEKF, but provide a new solution to the FT problem by "canceling out" dynamics and other disturbances that are spacecraft dependent. The IF is based on a linear transformation in output space (using measurements from both interferometers) that is invariant to dynamics. Finally, in the case of dim stars, when the FA and FT problems cannot be separated, this work offers a treatment in the form of a Multiple Hypotheses Tracking algorithm (MHT). The MHT entails a joint implementation of the Discrete Bayes Approach (DBA, see Ref. 1) to evaluate the *a posteriori* probabilities of hypotheses, and one of the tracking algorithms (EKF, NEKF, IF) to refine parameters for the most probable hypothesis. In Section 2.4 specific combinations of these tracking techniques are organized as strategies which are the basis of the analysis and simulation work.

In this paper, extensive parametric studies of the FT performance are carried out through the formalism of accuracy estimation in recursive filtering in the presence of various model mismatches. Moreover, the performance of the MHT algorithms is also studied analytically by the prediction tools presented in Ref. 1 for calculating the probability of detection. All this eliminates the need for time-consuming Monte Carlo simulations (especially in long-scale FT problems). Those simulations are performed only to validate the analytical predictions and investigate the robustness of various fringe tracking algorithms.

2. PHYSICAL MODEL OF FRINGE TRACKING

2.1 Instrument Configuration

The baseline configuration studied for the FT problem consists of two starlight interferometers, mounted at nearly a right angle, and a laser metrology system (see Refs. 2-4). Each interferometer "stares" at a target star with an off-axis angle δ, also referred to as in-plane pointing offset or the Optical Path Difference (OPD) angle, where the OPD = $L \cdot \delta$ and L is the instrument baseline. The instrument determines the actual angle $\gamma \approx 90°$, the angular separation between two widely separated stars, by measuring two OPDs δ^f (for the "first" interferometer) and δ^s (for the "second" interferometer) as well as by monitoring Δ, the articulation angle between the fiducial baselines of the two interferometers. We adopt the convention that during normal operations the "first" interferometer tracks a bright star ($m_{bol} \approx 10$), and the "second" interferometer tracks a star in the interval m_{bol} = 10-20. Accordingly, we will refer to the interferometers as "bright" and "dim". According to Refs. 2-4, the instrument measurement of the inter-stellar angle can be expressed in the form

$$\begin{aligned} \gamma &\approx 90° + \Delta + \delta^s - \delta^f + S_1 + S_2, \\ S_1 &\equiv \zeta^s - \zeta^f, \\ S_2 &\equiv \varepsilon^f \xi^f - \varepsilon^s \xi^s - \varepsilon^f \varepsilon^s \end{aligned} \tag{1}$$

where in addition to the articulation angle Δ and the two OPDs δ^f and δ^s, six other angles are involved. The angles ε^f and ε^s represent out-of-plane pointing offsets for the two interferometers. The other four angles represent the internal offsets,

i.e., the difference in angular orientation between the actual baseline and the fiducial baseline. The angles ζ^f and ζ^s are the in-plane internal offsets and the angles ξ^f and ξ^s are the out-of-plane internal offsets.

Equation (1) is an expansion of the exact nonlinear relation for the angular separation γ in a truncated Taylor series retaining the second-order terms. The laser metrology system enables the measurement of the articulation angle Δ with sub-microarcsecond accuracy. Thus, for purposes of the estimation process, Δ can be assumed known. The terms S_1 (first-order) and S_2 (second-order) are associated with biases (internal offsets) and must be inferred from post-measurement analysis of the interferometer and metrology data. In this paper we concentrate on the estimation of the difference $\delta^s - \delta^f$, which is directly connected with the interferometer measurements. It is important to note that we do not need to model the out-of-plane dynamics of the spacecraft since, with negligible loss of accuracy, the interferometer measurements can be considered as "in-plane" (see Ref. 3).

2.2 Channelled spectrum

The measurement equation for each interferometer, i.e., the equation which establishes the link between the average number of detected photons per detector and the OPD, will be used in the form (see Ref. 2) which accounts for the loss of visibility due to the OPD's motion:

$$\bar{Y}_{i\pm} = E[Y_{i\pm}] = \Delta t_{CCD} n(\nu_i) \Delta\nu_i \left[1 \pm \Lambda(\nu_i) \sin\left(\frac{2\pi L \nu_i}{c} \delta \right) \chi_i^{\nu} \chi_i^{t} \right] \qquad (2)$$

$$\text{where} \quad \chi_i^{\nu} = \operatorname{sinc}\left(\frac{\pi L \Delta\nu_i}{c} \delta \right), \quad \chi_i^{t} = \operatorname{sinc}\left(\frac{\pi L \nu_i}{c} \dot{\delta} \frac{\Delta t_{CCD}}{2} \right)$$

Eq. (2) is written for each i-th cell, where $\pm$ stands for plus and minus port respectively. There are nominally 512 CCD detector cells per beamsplitter output port at the focal plane (there are two ports, plus and minus, for a total of 1024 CCD detector cells). Also, Δt_{CCD} is the readout time interval; $n(\nu)$ is the envelope of the spectrum and is dependent on the stellar bolometric magnitude and stellar temperature; $\Delta\nu$ is the optical frequency bandwidth of cell i; Λ is the fringe visibility; ν is the optical frequency; L is the interferometer baseline; c is the speed of light; and, $L\delta$ is the optical path difference (OPD). The off-axis angle δ and its time derivative $\dot{\delta}$ are related to the middle of the CCD interval. The rate $\dot{\delta}$ is assumed to be constant over the CCD interval.

We will consider the situation when there are parametric and nonparametric uncertainties in the stellar spectrum. Parametric uncertainties (such as stellar bolometric magnitude m_{bol} and temperature T) are modeled as Gaussian variables while nonparametric uncertainty ($n(\nu)$) is modeled by a first-order linear shaping filter. A similar model of uncertainties will be exploited also for the visibility $\Lambda(\nu, t)$. Finally, the measurement equation includes the noise due to random photon arrivals and the electronic readout noise. The actual number of photons detected in each i-th cell (of the "+" or "-" port) at one readout is a Poisson random variable with mean $\bar{Y}_{i\pm}$. The DBA algorithm directly accounts for this fact (see Ref. 1). For Kalman-type estimators (EKF, NEKF, IF), it is necessary to perform a Gaussian approximation of the Poisson distribution.

2.3 Model of spacecraft dynamics

The end-to-end model of the POINTS spacecraft systems for the FT task (see Refs. 4-6) includes the dynamic model of the spacecraft with the Attitude Control System (ACS), the model of the instrument flexibility, the mechanism of harmonic disturbances in the Reaction Wheel Assembly (RWA), and the characteristics of the Rate Gyro (RG) measurement noise. A new element of the current POINTS design is the Fine Pointing and Isolation System (FPIS). Two major scenarios in modelling the SC systems will be considered: 1) without FPIS, and 2) with FPIS. This approach will investigate the pure effect of the FPIS in terms of enhancing the performance of the interferometer instrument.

According to Refs. 4, 5 in-plane angular motion is modeled by a one degree-of-freedom dynamical system consisting

of a rotational inertia that is acted on by a torque assumed to be external (i.e., we ignore the RWA dynamics). In order to obtain a preliminary model of the disturbance environment for the POINTS spacecraft, it was decided to closely follow the characterization of the noise for the Hubble Space Telescope (HST). In the simulation of the spacecraft with an attitude control system, the gyro is modelled as a perfect measurement of the attitude rate plus additive white noise. From the available data on rate gyros used on the Hubble Space Telescope (Ref. 6) we extracted a one-sided PSD level for an assumed white noise source into the gyro rate measurements of 1.6×10^{-5} (arcsec/sec)^2 /Hz (budget level) or 8.0×10^{-5} (arcsec/sec)^2 /Hz (capability level). To model the RWA sinusoidal disturbances, we will follow the results of Refs. 8 and 9. For radial torques, axial forces, and radial forces, the amplitudes of the disturbance components are functions of the square of the wheel speed. Also, a white noise model for RWA disturbances is used to provide intensive multi-parametric studies.

The design of the attitude control system for the simplified one-axis, rigid model of the POINTS spacecraft follows standard practice, in particular, a PD (position plus derivative) controller is used to maintain attitude stability in the presence of disturbances. The RG measurement is used in the derivative part of the PD controller. For simplicity, we assume that the measurement needed for the proportional part of the PD controller is provided by a direct attitude sensor such as the Fine Guidance Sensors (FGS's) used in the HST. The assumed FPIS attenuates the OPD dynamics up to 40 db in the frequency range > 0.4 Hz and has a linear slope of -20db/decade in the range 0.004 - 0.4 Hz.

2.4 Model architectures for fringe tracking

Using the building blocks of Section 2.3, we are able to form a model for the fringe tracker that takes the form of a state-space discrete-time system (see Ref. 6):

$$\begin{aligned} x_{k+1} &= A x_k + B u_k + F \xi_k \\ y_k &= g_k(x_k) + \eta_k \end{aligned} \tag{3}$$

where k is the discrete time index (corresponding to the middle of the CCD intervals); x is the (n × 1) state-vector; u is the (n_u × 1) deterministic disturbance (sinusoidal disturbance from RWA); ξ is the (n_ξ × 1) stochastic disturbance (RG noise); y is the (m × 1) measurement vector (readouts in each cell of the two interferometer ports); η is the (m × 1) Gaussian measurement error (comprised of the photon noise and electronic readout noise); A,B and F are (n × n), (n × n_u), and (n × n_ξ) matrices, respectively, describing the linear dynamic characteristics; g is the vector function (m × 1) representing the measurement as a nonlinear function of the OPD and model parameters.

The composition of the state vector x_k depends on the particular FT scenario. The following logical schemes formalize a set of possible scenarios. First, the scenario is defined by the strategy for fringe tracking, i.e., by what is going to be estimated and how:

Strategy #1:	Tracking "bright" OPD by EKF (NEKF)
Strategy #2:	Tracking "bright" and "dim" OPDs independently by EKF (NEKF)
Strategy #3:	Tracking "bright" OPD and angular separation by EKF (NEKF)
Strategy #4:	Tracking angular separation by IF

Second, the scenario is defined by the composition of the spacecraft/instrument model, which consists of various combinations of the following blocks:

Block #1:	With (1) or without (0) SC + ACS
Block #2:	With (1) or without (0) FPIS
Block #3:	With (1) or without (0) instrument flexibility
Block #4:	With (1) or without (0) model parameters

The corresponding scenario can be numerated now, for example, as 4(1.1.1.0), which means that the invariant filter uses the dynamic model with the FPIS, with the instrument flexibility, without the uncertainties in the model parameters (spectrum, visibility).

The first two strategies are straightforward. The third strategy (tracking "bright" OPD and angular separation) assumes that the information from the "bright" interferometer can be used for tracking a "dim" star. In this case, the augmented state-vector x includes the state vector x^f for the "bright" ("first") interferometer and one more component which is the angular separation γ. The OPD angle δ^s for the "dim" ("second") interferometer can be expressed through the "bright" OPD angle δ^f and the angular separation γ by using Eq. (1) and ignoring the terms S_1 and S_2. The fourth strategy (tracking angular separation by the IF) provides the possibility of "canceling out" the block x^f in the augmented state-vector x, and, thus, having the scalar FT problem with the "state-vector" $x = \gamma$. The invariant filter approach will be explained in Section 3.2.

3. PROPOSED SOLUTION ALGORITHMS

3.1 Kalman-type filters (EKF and NEKF)

We use the EKF equations in a standard way as recommended in Refs. 10, 11 for the discrete-time system of Eq. (3). However, due to the highly-nonlinear nature of the interferometer's measurements, the EKF may be divergent. That is why a nonlinear Kalman-type filter (NEKF) was developed. A detailed description of the NEKF is given in Refs. 6, 12, but in this paper we introduce only the main idea. It is based on the following transformation for the nonlinear filtering problem (Eq. (3)):

$$y_{ki} = (1 \quad 0....0)\begin{pmatrix} z_{ki} \\ x_{ki} \end{pmatrix} + \eta_{ki}, \quad k = 1,...,N; i = 1,...,m \tag{4}$$

where the new augmented state vector consists of the mean of y_{ki}, $z_{ki} = g(x_{ki})$, together with the state vector x_{ki} (the index i denotes the state vector x_k which corresponds to the current measurement component y_{ki}); η_{ki} is the i-th component of the measurement error vector η_k.

In these new coordinates Eq. (4) becomes linear and has a particular structural advantage which will be exploited in the filter design. Now all nonlinearities are "isolated" in the dynamics of the system for the augmented state-vector. In other words, the measurement nonlinearities are interpreted as nonlinear dynamics in the augmented system. As a result, the NEKF consists of two steps: prediction (nonlinear) and update (linear). At the prediction step a problem of nonlinear statistical analysis is solved to evaluate the *a priori* characteristics (thereby, nonlinearity $g(\cdot)$ can be approximated by 2nd or 3rd-order polynomials). At the update step the linear Kalman filter is used to evaluate the *a posteriori* characteristics.

3.2 Invariant filter (IF)

The installation of the FPIS helps to achieve instrument stability (in the presence of dynamic disturbances on-board) sufficient to make readouts at large time intervals without loss of visibility. However, it is still problematic to reach the specified accuracy in the estimation of the angular separation between two stars (5 microarcseconds or 2.4×10^{-11} rad). The main reason is that for the few minutes provided for the total observation it is practically impossible to filter out the undesired dynamics since they, even attenuated by the FPIS, are 2-3 orders of magnitude larger than the specified accuracy and their correlation time is less than the observation interval (under current assumptions). Consequently, it would be beneficial to find a way of "canceling out" dynamics in the fringe tracking process. This can be done through the Invariant Filter (IF) which provides an effective way to combine the measurement information from the four telescopes of the two interferometers.

Let us examine the main concept behind the IF for the simplest case when the "first" ("bright") and "second" ("dim") interferometers have the same CCD readout interval and the loss of visibility due to dynamics can be neglected. Assume that the FA problem has already been solved and that the OPDs for both interferometers are known with sufficient accuracy so that it is possible to linearize the measurement equation. Let the linearized measurements have the following form:

$$\begin{aligned} \Delta y^f &= C^f \Delta\delta^f + \eta^f \\ \Delta y^s &= C^s(\Delta\gamma + \Delta\delta^f) + \eta^s \end{aligned} \tag{5}$$

Here, the index k, indicating the readout number, is omitted for simplicity. The notation Δ means deviation of the actual magnitude from its reference value. The first-order sensitivity matrix C is calculated for each interferometer in the vicinity of its reference OPD angle.

The conventional approach to estimating the target parameter $\Delta\gamma$ would be to develop a dynamical model for the "remaining" OPD angle $\Delta\delta^f$ and then to implement the EKF to filter out the time varying systematical error $\Delta\delta^f$ along with the measurement noise. The IF offers an alternative approach that does not require the development of a dynamical model and that estimates the angular separation $\Delta\gamma$ directly and more accurately. This is done through a special transformation of the outputs from both interferometers.

Introduce a linear combination of the interferometers' measurements:

$$\Delta y^{inv} = \beta^f \Delta y^f + \beta^s \Delta y^s \tag{6}$$

where β^f and β^s are arbitrary matrices of the size (m × m). Note that in the general case the size can be (K·m × K·m) where K is the number of readouts which form the blocks of the measurement vector Δy. By requiring that the matrices β^f and β^s satisfy the condition of invariance:

$$\beta^f C^f + \beta^s C^s = 0 \tag{7}$$

the transformed observation Δy^{inv} is invariant with respect to the dynamical parameter $\Delta\delta^f$, i.e., depends only on the target parameter $\Delta\gamma$:

$$\Delta y^{inv} = \beta^s C^s \Delta\gamma + \eta^{inv}, \quad \eta^{inv} = \beta^f \eta^f + \beta^s \eta^s \tag{8}$$

It is clear that the parameter $\Delta\gamma$ is observable from the measurement Δy^{inv} for non-trivial β^s and β^f. It should also be clear that the performance of the associated EKF will depend on the choice of invariant transformation. There is a compromise between the sensitivity and the noise characteristics in the invariant measurement (Eq. (8)). Mathematically, finding the optimal β^f and β^s takes the form of a Riccati equation control problem for the covariance matrix (in this case variance) of the parameter $\Delta\gamma$. This long-standing problem was first solved analytically in the '80s (see Ref. 13). The solution is based on exploiting the analytical properties of the Riccati equation in a nontraditional manner, namely in the form of sufficient projections of the Hamiltononian system. For the current problem, the strictly optimal solution involves a boundary-value problem. Analysis shows, however, that it is possible to use a near-optimal solution which is simple and, at the same time, appropriately accounts for both the sensitivity and the noise characteristics in Eq. (8).

The near-optimal solution requires that the cells of each interferometer be rearranged in the order of their information content which is defined as $F_i = C_i^2 \Theta_{\eta_i}^{-1}$ where F_i is the Fisher "matrix" for each cell. This rearrangement makes the cells in both interferometers more "compatible" for the invariant transformation (Eq. (6)). Note, that this rearrangement can also be done for the case of multiple readouts, but simulations show that it is sufficient to perform the "cancellation" of dynamics at each single readout. After the cells' rearrangement, the matrices β^f and β^s can be chosen to be of diagonal form where each element of the diagonal (for each cell) is defined as

$$\beta_i^s = 1, \quad \beta_i^f = -\frac{C_i^s}{C_i^f} \tag{9}$$

Effectively, the optimized IF enables the two interferometers to work as one four-telescope device to provide a quiescent environment for observations of the inte- stellar angle.

The practical implementation of the IF requires that we address the differing sampling rates in the dim and bright interferometers as well as the problem of obtaining initial estimates of both OPDs in the linear range. At last , in reality there are two situations when residual dynamics can destroy the ideal dynamic-invariance of the IF and, thus, degrade to some extent the estimation accuracy. The first situation arises when uncertainties in the OPD are large enough ($> 5 \times 10^{-8}$ rad) and the higher order terms in the measurement equation should be accounted for. The second situation takes place when there are parametrical (θ) and nonparametrical uncertainties in the sensitivity matrices $\Delta C^f(\theta)$ and $\Delta C^s(\theta)$ caused, for example, by model uncertainties (in visibility, in the spectrum, due to a lack of physics, etc.). In this case the invariant measurement will depend on the dynamics coupled with the uncertainties in C (second-order effect). In all these situations the dynamics have a second-order effect on the FT performance and can be treated through nonlinear filtering by the NEKF. All of the above issues are addressed in detail in Ref. 6.

3.3 Multiple hypotheses tracking (MHT)

In the case when the "second" star is fairly dim, the difference between the FA and FT problems is blurred. During the tracking process it is no longer possible to say that the star is detected within the specified FA interval ($< 10^{-7}$ rad) with probability equal to 1. The mechanism of "loss of lock" (LOL) in the photon-starved situation was identified in Ref. 1. Its roots are in the physics of the interferometer's measurement function, namely in the fact that each "true" OPD angle has a few "mirror" OPD at which the spectra are quite similar to the "true" one. This leads to a Multiple Hypotheses Tracking (MHT) problem, which entails that the fringe tracker provide the *a posteriori* probabilities for the candidate hypotheses (approximate locations of the "mirror" OPD angles) and the more accurate refined OPD angle estimates for selected hypotheses. This is the most natural and effective representation of the processed information, better than providing a single (averaged) estimate for the OPD (or the angular separation) along with its standard deviation (STD) as the accuracy characteristic.

Of several possible MHT architectures (see Ref. 5) we present only the simplest one in this paper. The DBA with a low resolution grid in the OPD angular range (10^{-8} - 5×10^{-8} rad) is run for the entire observation interval to provide the *a posteriori* probabilities for the angular separation γ; then a Kalman-type fringe tracker (EKF, NEKF, IF) processes the data again to refine the estimate of γ in the vicinity of the most probable hypotheses. In this case, the reference OPD for the dim star is restored from the estimates of the "bright" OPD (time-varying) and the angular separation γ (constant). The DBA for the multiple hypotheses tracking strategy has conceptually the same form as in Ref. 1. Its invariant (to dynamics) implementation is also possible by using Eq. (8) and evaluating the Poisson distribution of the measurement errors.

4. ANALYSIS

4.1 Analysis for bright stars

In the case of bright stars, when the OPD is detected within a relatively small range of uncertainty, one can analyze the tracking accuracy by using only the covariance relations of the Kalman-type filters (EKF, NEKF, IF). Moreover, it is sufficient to study their steady-state regime (if it exists) to reduce the calculations necessary for multi-parametric studies. Strictly speaking, this involves some approximations for two reasons. First, the covariance equation of the filter is coupled with the estimate equation due to the original nonlinearity of the measurement equation. Second, the sensitivity matrices in the filter equations are time-varying. This paper treats both situations by introducing the so-called generalized measurement, which is the estimate of the OPD after one readout. In Ref. 1 the accuracy of the estimate after one readout was analyzed. Its dependence on the OPD is characterized by a drop in accuracy in two small regions around $\pm$ 0.6785 $\times$ 10^{-7} rad; for the remaining OPDs in the range of study this dependence is quite flat. As a result, one can use the average

accuracy of the generalized measurement:

$$\bar{\sigma}_\delta^2 = \int_{-\infty}^{\infty} f(\delta)\sigma_\delta^2(\delta)d\delta \qquad (10)$$

where $f(\delta)$ is the density of probabilities for the OPD angle δ calculated from the dynamic stochastic model; and, $\sigma_\delta^2(\delta)$ is the STD of the generalized measurement at the fixed δ. The calculation of the STD σ^2_δ is based on one iteration of the EKF's covariance equation. After the STD of the generalized measurement is computed, one can use the conventional analysis of the steady-state filtering accuracy in the linear system with the linear (position) measurement.

4.2 Analysis for dim stars

In the photon-starved case, the interpretation of the tracking accuracy differs from the "bright" situation. As mentioned above, in this case the construction of "the average estimate + accuracy bounds" is too rough since the *a posteriori* density of probabilities is not Gaussian (see, Ref. 1). Remember that loss of lock (LOL) occurs due to misidentifying the "true" OPD for the "mirror" OPDs, which have spectra similar to the "true" one (see Ref. 1). Since the "mirror" OPDs are quite distant from the "true" OPD ($>10^{-7}$ rad), it is possible to characterize the performance of the MHT algorithm by two criteria: 1) the probability of detecting the "true" OPD within the given interval (10^{-7} rad); 2) the STD of the "local" error in OPD, i.e., the width of the *a posteriori* density peak at the "true" OPD.

The evaluation of the "local" STD can be performed exactly in the same way as it was described in Section 4.1 for tracking "bright" stars by the Kalman-type filter. It should be noted that the "local" STD is the lower bound for the total STD which accounts also for the "global" errors, i.e., the side peaks of the *a posteriori* density at the "mirror" OPDs. In other words, the "local" accuracy analysis is a dynamic form of the Cramer-Rao lower bound for the estimation error in nonlinear systems. The evaluation of the probability of detection is based on the analytical approach presented in Ref. 1. For the case considered, the detection (FA) problem, as mentioned above, is "static" in terms of the angular separation γ, but its "dynamic" nature still remains since the measurement properties depend on the changing OPD. To account for this situation one can calculate the average probability of detection (due to dynamics):

$$p_d = \int_{-\infty}^{\infty} f(\delta)p_d(\delta)d\delta \qquad (11)$$

where $p_d(\delta)$ is the detection probability at the fixed OPD angle δ; and $f(\delta)$ is the density of probabilities for the OPD due to its dynamics. Eq. (11) is the formula of full probability and is similar to the averaging carried out in Eq. (10).

5. RESULTS

Four classes of estimation algorithms were studied for different scenarios of the FT problem. Those scenarios were defined in Section 2.4 and dubbed by the sequence of numbers *(*.*.*.*). As mentioned earlier, two major approaches are used to study the POINTS performance: Monte Carlo simulation and analytical prediction. The preference is given to the analytical approach in order to enable intensive and quick multi-parametric studies of the performance.

5.1 Analytical studies

Consider the situation of tracking a "bright" star by one interferometer using the EKF in the dynamical environment due to RWA disturbances and RGA noise. The corresponding scenario of the FT problem has the number 1(1.0.0.0). To simplify the multi-parametric study of the FT performance, assume that the RWA disturbance is modelled by the equivalent white noise. Figure 1 (upper plot) illustrates the dependence of the steady-state FT performance on the intensity of the disturbance and white noise. Both nominal intensities are varied from zero to the nominal value by a common scaling parameter k ($0 < k < 1$). The results are presented for different intensities of the readout noise ($\sigma_{noise} = 0 - 4$). It should be noted that the accuracy of a single readout plotted on the upper part of Figure 1 depends on k due to the averaging procedure (Eq. (10)).

Accordingly, there is a small peak of the OPD error at k = 0.05, since the steady-state variation in the OPD angle (see the bottom plot of Figure 1) entails more frequent stay in the two "worst" near-zero OPD regions.

As can be seen from the analysis performed, the steady-state error in OPD angle is two orders of magnitude larger than in the specified accuracy of 5 microarcseconds, and, more importantly, decreasing the intensity up to 10^2 - 10^4 times (k = 0.01 - 0.1) does not provide a significant improvement in the performance. The latter fact helps to predict that just using a stabilization system which attenuates motion of the OPD angle up to 2 orders of magnitude is still not the ultimate solution to the problem. The explanation for this significant "dynamic" degradation of accuracy (in the OPD angle and its drift) is quite simple. The OPD angle changes in the region of 10^{-9} - 10^{-6} rad (see Figure 1, bottom plot) and the correlation time of its dynamics is a few seconds. The rate at which stellar measurements reduce the uncertainty in the OPD estimate is too "slow" to follow this motion.

Figure 2 provides a general comparative analysis of the most interesting scenarios in estimating the angular separation. Three of the strategies described in Section 2.4 are considered: strategy 2 - tracking "bright" and "dim" OPDs independently; strategy 3 - tracking "bright" OPD and angular separation; strategy 4 - tracking the angular separation directly (i.e., using the IF). In addition, these scenarios will include interesting compositions of the state vector (see Section 2.4). The performance study accounts for the SC + ACS dynamics, the FPIS, and model uncertainties in the spectra and visibility. Note that the model uncertainties make the matrix of sensitivities C uncertain and, thus, robustness of the IF to the residual second-order dynamical effects can be investigated.

The FT performance is studied with respect to the bolometric magnitude of the "second" star assuming that the "first" star is bright (m_{bol} = 10). This will allow us to investigate the general feasibility of high-precision interferometry. Figure 2 presents the results for σ_{noise} = 3 and no cell grouping (for either interferometer). Taking into account the fact that the performance study involves dim stars, the performance is represented by two criteria: 1) the probability of detecting the "true" OPD within 10^{-7} rad (plotted in the lower plot of Figure 4); and 2) the STD of the "local" error in OPD angle (plotted in the upper plot of Figure 4). These two criteria for performance provide more information on the mechanism of the estimation error in the case of tracking dim stars than the total STD. The "local" STD in the case of dim stars is the Cramer-Rao lower bound for the total STD. However, in the case of bright stars (or more precisely, for observation times which provide a detection probability close to 1), the "local" STD approaches the exact total STD. It should be noted in Figure 2 that the explicit dependence of the FT performance on OPD is "eliminated" through the averaging due to dynamics (see Eqs. (10) and (11)). Using the presence of dynamics in the model helps to explain the fact that the FT performance ("local" STD) exhibits saturation for dim stars. The performance simply returns to the level of the OPD angles' variations due to dynamics since the photon-starved observations are lacking sufficient information to improve the estimates. All results of Figure 4 are computed for the given observation interval, since there are no steady-state regimes for strategies 3 and 4 (strategy 2 is treated using the time-varying EKF covariance equations).

The information on the details and parameters is displayed in Figure 2. We will characterize only some principal tendencies encountered in this multi-parametric and multiple-algorithm performance study. First, the second strategy of the FT problem, i.e., when the "bright" and "dim" OPDs are estimated independently and the estimation variances are added up, is notoriously not optimal and does not meet the accuracy specifications. Second, better accuracy is achieved by using the third strategy, i.e., tracking the "bright" OPD and the angular separation. As mentioned in Section 2.4, the estimation of the angular separation $\Delta\gamma$ becomes "static" and the "first" OPD $\Delta\delta^f$ plays the role of time-correlated systematic error. It is interesting to note that for the case when the "second" star is fairly dim the effects of the error in $\Delta\delta^f$ is negligible since this error is on the order of 10^{-9} rad, while the achievable $\Delta\gamma$ uncertainty, even in the static case, is larger than 10^{-8} rad. In fact, in this case the EKF's performance for strategy 3 approaches the "static" limit. However, in the case of "bright" second stars, the FT performance hits a "floor" at a level which is approximately one order of magnitude off from the "static" accuracy. The physical explanation of this fact is the following. It is impossible, for the given observation time (150 sec.), to filter out the large (>10^{-9} rad) systematic error $\Delta\delta^f$ which has a correlation time of a few seconds. This means that approaching the accuracy level of 5 microarcseconds under conditions of real disturbances is a serious problem even for bright stars. This problem can be solved by the IF, which "cancels out" dynamics before they need to be modelled and then filtered out. The IF performance practically approaches the "static" EKF accuracy in the case when there are no uncertainties in the sensitivity matrix C. However, when those uncertainties do take place, the IF is quite robust due to its ability to filter out the second-

, order terms $\Delta C \cdot \Delta\delta^f$

Figure 2 (the lower plot) also provide a study of the detection probability, but for the given parameters this probability is not equal to 1 only for fairly dim stars and for the case when $\sigma_{noise} = 3$ and no cells are grouped. It is interesting to note that the analytically predicted probability of detection is nearly the same for the different scenarios considered. This is explained by the fact that the global nonlinear mechanism of detecting a star is the same and is analyzed under the same statistical conditions (Gaussian continuous model).

5.2 Simulation studies

Six additional points for Figure 2 were obtained through Monte Carlo simulation of the FT process. One hundred realizations were carried out for each simulation variant in order to generate a statistically significant set. Even in this case, the entire simulation process took about 100 hours of CPU time (the corresponding analytical predictions were 500-1000 times cheaper). In all cases the scenario 4(1.1.0.0 was used, i.e., the invariant transformation for direct estimation of the angular separation γ was assumed. Three points for m_{bol} = 11,13 and 15 correspond to the simulation of the EKF, the other three points for m_{bol} = 12, 19 and 20 correspond to the DBA which uses the genetic Markov chain to discretize the OPD interval with sufficient accuracy at the most probable hypotheses (see Ref. 1). As can be seen from the simulation results displayed in Figure 2, analytical prediction of the FT performance for the EKF is quite consistent with the actual EFK's accuracy under conditions of real Poisson distributions. At the same time, the actual FT performance achieved by the DBA is noticeably better for dim stars. This is explained by the fact that the DBA handles the Poisson photon arrivals in an exact manner which is important in the photon-starved situation.

Figure 3 presents one realization of a single Monte Carlo process which illustrates the DBA's mechanism for detecting the angular separation between stars (or the difference of their OPD angles). Unlike the "multiple" Monte Carlo runs shown in Figure 2, the results correspond to m_{bol} = 18 and Δt_{CCD} = 0.01 and 0.1 sec (for bright and dim stars, respectively). As could be expected in the case of nonlinear systems, the estimate and its accuracy significantly depend on how favorable or not is each random realization. The DBA is the most sensitive of the algorithms presented to extract the maximum information from a particular observation. The estimate based on the maximum of the *a posteriori* density of probabilities is capable of capturing the "true" angular separation after a shorter observation time than what is possible with the estimate based on the mean of the *a posteriori* density. Moreover, the second and third peaks of the *a posteriori* density provide additional information, since in a fairly "dim" case it is better to identify a few probable locations of the dim star rather than have a rough "averaged" estimate.

Figures 4 and 5 illustrate the mechanism of tracking by a Kalman-type filter and compare its linearized (EKF) and nonlinear (NEKF) versions. Figure 4 demonstrates the main advantage of the 3rd-order NEKF over the EKF for an initial uncertainty of 1×10^{-7} *rad*. As can be seen, the EKF (retaining only 1st-order terms in the measurement nonlinearity) diverges, i.e., the error bounds (3-sigma) do not contain the true OPD. The attempt to make the filter more robust to the even (2nd-order) nonlinear effect fails again. Finally, the nonlinear filter with the 3rd-order term is able to capture the fundamental characteristic of the odd nonlinear function Eq. (2) and provides stable tracking. Figure 5 illustrates another effect of the nonlinear nature of the interferometric estimation problem. When the OPD angle passes through two areas of low sensitivities in the vicinity of the two "worst" OPD angles with initial uncertainties on the edge of the linear range (5×10^{-8} rad), the EKF loses its convergence. It occurs due to the fact that the information starved linearized measurements cannot compensate for disturbances and, as a result, uncertainty in the OPD grows beyond the linear range. At the same time, the 3rd-order NEKF is convergent. As we have seen, the advantage of implementing the NEKF is two-fold. First, it is possible to start tracking from a broader range of uncertainty in the OPD (up to 1×10^{-7} *rad*) and model parameters. Thus we conclude that the robustification of the FT process to nonlinearities, achieved by the NEKF, can be of great value.

6. CONCLUSIONS AND RECOMMENDATIONS

Dynamics is the major factor in preventing the FT performance from reaching the specified accuracy of 5 microarcseconds in the estimation of the angular separation between two stars. (Inclusion of the FPIS provides high optical stability of the instrument but it is not sufficient to bring the FT performance to the specified accuracy level even for bright stars.) The remaining gap of one (or more) order(s) of magnitude is explained by the fact that the dynamics, even attenuated,

are still 2 to 3 orders of magnitude larger than the required level of accuracy. This makes it difficult to track each OPD or to filter out the OPD motion from the angular separation for the given observation time. The treatment of this situation is provided by IF which performs an invariant transformation of the outputs from both interferometers in such a way as to "cancel out" dynamics before they need to be modelled and filtered out. This uses a simpler model of the FT problem and practically achieves the "static" accuracy. A high robustness of the IF to possible residual second-order dynamical effects (e.g., due to uncertainties in the measurement sensitivities) was confirmed through analysis and simulations. It can thus be concluded that the IF for FT promises to allow space-borne interferometry to reach its full potential by providing the ideal "undisturbed" space environment wherein to observe the universe.

There is a need to robustify the fringe tracking process by accounting for the higher-order nonlinearity terms of the measurement equation. This should be done for three reasons. First, to start tracking from relatively large ($\sim 10^{-7}$ rad) uncertainties in OPD angle. Second, to prevent the filter's divergence whenever there is a loss in OPD angle accuracy (e.g., due to passing through the "worst" OPD angle areas or due to "unmodelled" factors). Third, to properly handle uncertainties in the model parameters (e.g., optical visibility). The NEKF, developed in the framework of high-precision interferometry, offers the most effective approach to handle the third-order Taylor terms from the measurement nonlinearities with minimal increase (1.2 - 1.5 times) in computational expenses compared to the linearized EKF. As a result of implementing the NEKF, the radius of the fringe tracker's convergence is expanded between 2 and 3.5 times.

The FT performance in tracking dim stars can be substantially increased by taking advantage of the discrete Poisson distribution of photon arrivals. In this case, by using the corresponding Bayes algorithm (DBA), it is possible to track dimmer (by 1 to 1.5 bolometric magnitudes) stars with the same performance as in the case of the NLS. The MHT concept developed in this work provides a comprehensive and optimal solution for the processing of the stellar measurements in the photon-starved regime. In the general case, the processed information is transformed into the *a posteriori* density of probabilities (usually, with a few peaks). The capabilities of the DBA are then fully exploited through the use of "genetic" discretization of the OPD angular range to achieve the specified resolution, without resorting to time-consuming gridding of the wide angular range. In some other cases, when it is possible to sacrifice some accuracy in the interest of a less computationally expensive algorithm, the MHT algorithm can be a hybrid of the low-resolution DBA (used to filter out spurious hypotheses) and a Kalman-type filter (EKF, NEKF, IF) to refine the FT performance.

7. ACKNOWLEDGEMENTS

This work has been conducted under NASA/JPL Phase II SBIR contract #NAS7-1248, entitled Estimation Tools for Precision Interferometry.

8. REFERENCES

1) Padilla, C.E., Karlov, V.I., Tsitsiklis, J.N., Li, J., Reasenberg, B., Chun, H.M.
"The Problem of Fringe Acquisition in High Precision Space-based Interferometers", #2477-06, SPIE Conference, Orlando, FL, 1995

2) Reasenberg, R.D., Babcock, R.W., Noecker, M.C., Philips, J.D.
"POINTS: the First Small Step" (Invited Paper). Proceedings of the SPIE on Spaceborne Interferometry, Orlando, Florida, April, 1993.

3) Reasenberg, R.D., Babcock, R.W., Chandler, J.F., Gorenstein, M.V., Huchra, J.P., Pearlman, M.R., Shapiro, I.I., Taylor, R.S., Bender, P., Buffington, A., Carney, B., Hughes, J.A., Johnstron, K.J., Jones, B.F., and Matson, L.E., 1988, "Microarcsecond optical astrometry: an instrument and its astrophysical applications." Astron. J., **32**, pp. 1731-1745.

4) Schumaker, B.L., Ulvestad, J.S., Agronin, M., Chen, G-S, Ledeboer, W.D., Melody, J.W., Noon, D.E., Peng, C-Y.
"POINTS: Spacecraft Studies." 1992-1994 Progress Report, Jet Propulsion Laboratory, California Institute of Technology, June, 1994.

5) Padilla, C.E., Chun, H.M., Matson, L., Reasenberg, R.D.

"Fringe Tracking Filters for Space-Based Interferometers". Proceedings of SPIE on Spaceborne Interferometry, Orlando, Florida, April 1993.

6) Padilla, C.E., Karlov, V.I.
"The Problem of Fringe Tracking in High Precision Space-Based Interferometers: Part I - Parametrical Studies," Technical Memorandum ETPI TM195, MOM495, February, 1995

7) Private communcation with Dr. Kenneth F. Tompetrini, Senior Program Manager, Bendix Guidance & Control Systems, a division of Allied-Signal Aerospace Company, Teterboro, NJ, 17608-1173.

8) Hasha, M.D.
"Reaction Wheel Mechanical Noise Variation," LMSC EM SSS 218, June 1986.

9) Melody, J.W. and Briggs, H.C.
"Analysis of Structural and Optical Interactions of the Precision Optical Interferometer in Space (POINTS)", Technical Memorandum 343-93-165, Jet Propulsion laboratory, California Institute of Technology, May, 1993.

10) Gelb, A., Editor
Applied Optimal Estimation, The MIT Press, Cambridge, Massachusetts, 1989.

11) Jaswinsky, A.H.
Stochastic Processes and Filtering Theory, Academic Press, New York, NY. 1970.

12) Karlov, V.I., Padilla, C.E., Chun, H.M.
"Nonlinear Kalman-type Filter for High Precision Interferometry", to be submitted to AIAA Journal of Guidance, Control and Dynamics.

13) Malyshev, V.V., Krasilçhikov, M.N., and Karlov, V.I.
Optimization of Observation and Control Processes, AIAA Education Series, 1992.

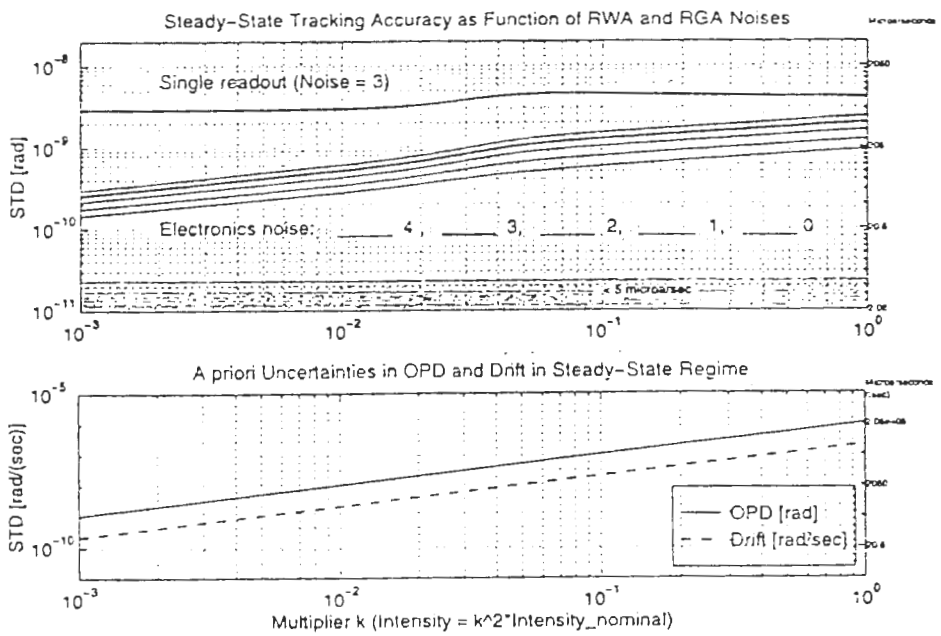

Figure 1 Dependence of Tracking Accuracy on Intensity of RWA and RGA Noises

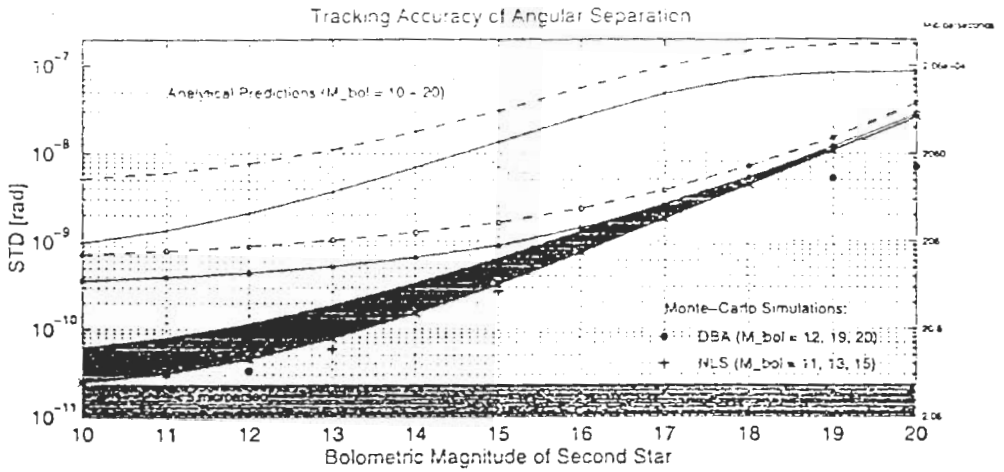

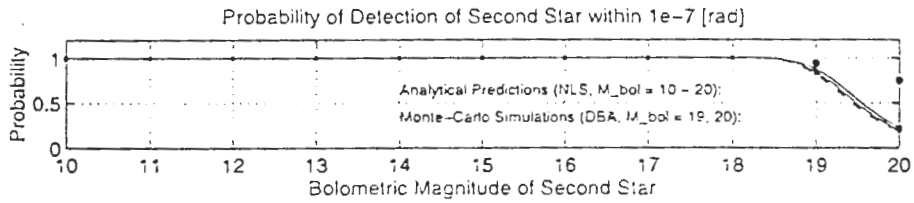

Filter & Model:

- Scenario 2(1.0.1.0.0): EKF, SC+ACS+flexibility, Sinusoidal RWA disturbance at 8.63 Hz, RGA noise
- Scenario 3(1.0.1.0.0): EKF, SC+ACS+flexibility, Sinusoidal RWA disturbance at 8.63 Hz, RGA noise
- Scenario 2(1.1.0.0.0): EKF, SC+ACS+FPIS, Sinusoidal RWA disturbance at 8.63 Hz, RGA noise
- Scenario 3(1.1.0.0.0): EKF, SC+ACS+FPIS, Sinusoidal RWA disturbance at 8.63 Hz, RGA noise
- Shadow * Scenario 4(1.0.1.1.0): IF, SC+ACS+flexibility, Sinusoidal RWA disturbance at 8.63 Hz, RGA noise, 0-20%-Uncertainty in C
- Scenario 4(1.0.1.0.0): IF, SC+ACS+flexibility, Sinusoidal RWA disturbance at 8.63 Hz, RGA noise, Known C

Figure 2 Comparison of EKF and IF

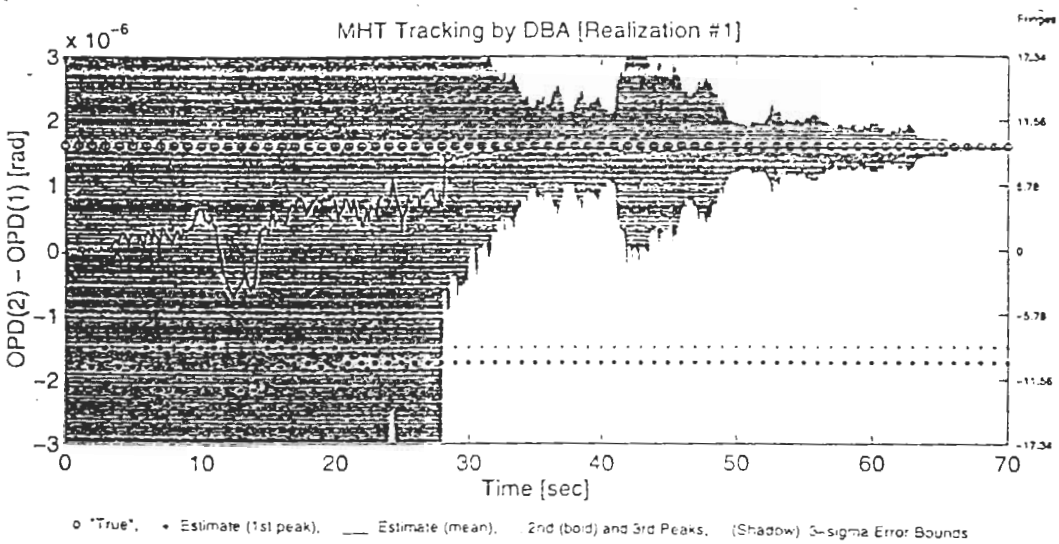

Figure 3 Multiple Hypotheses Tracking by DBA

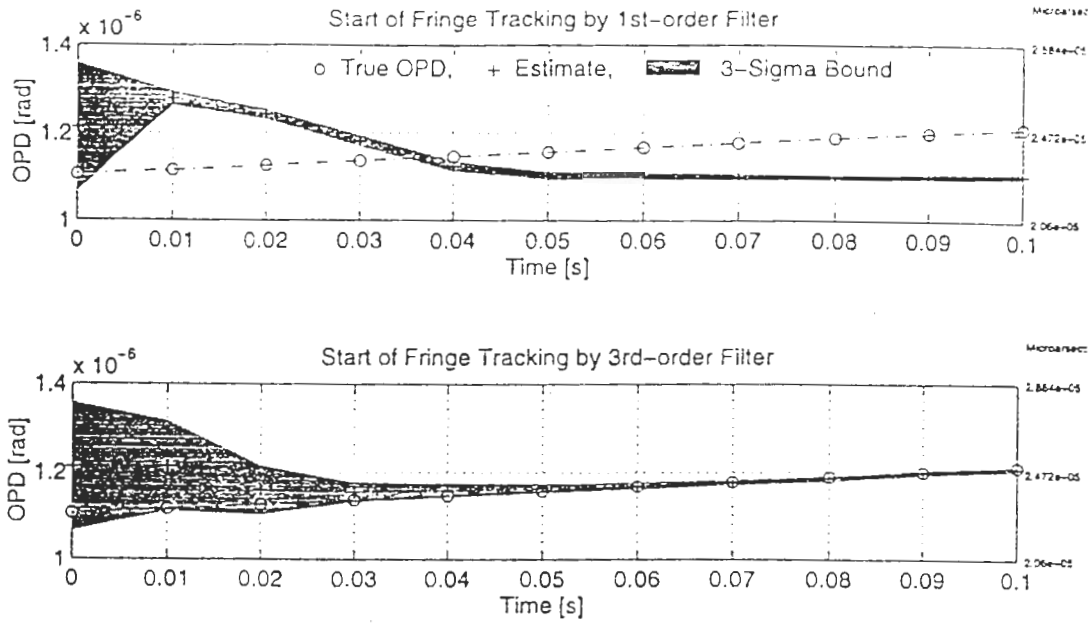

Figure 4 Initialization of EKF and NEKF from Broad Range of Uncertainties

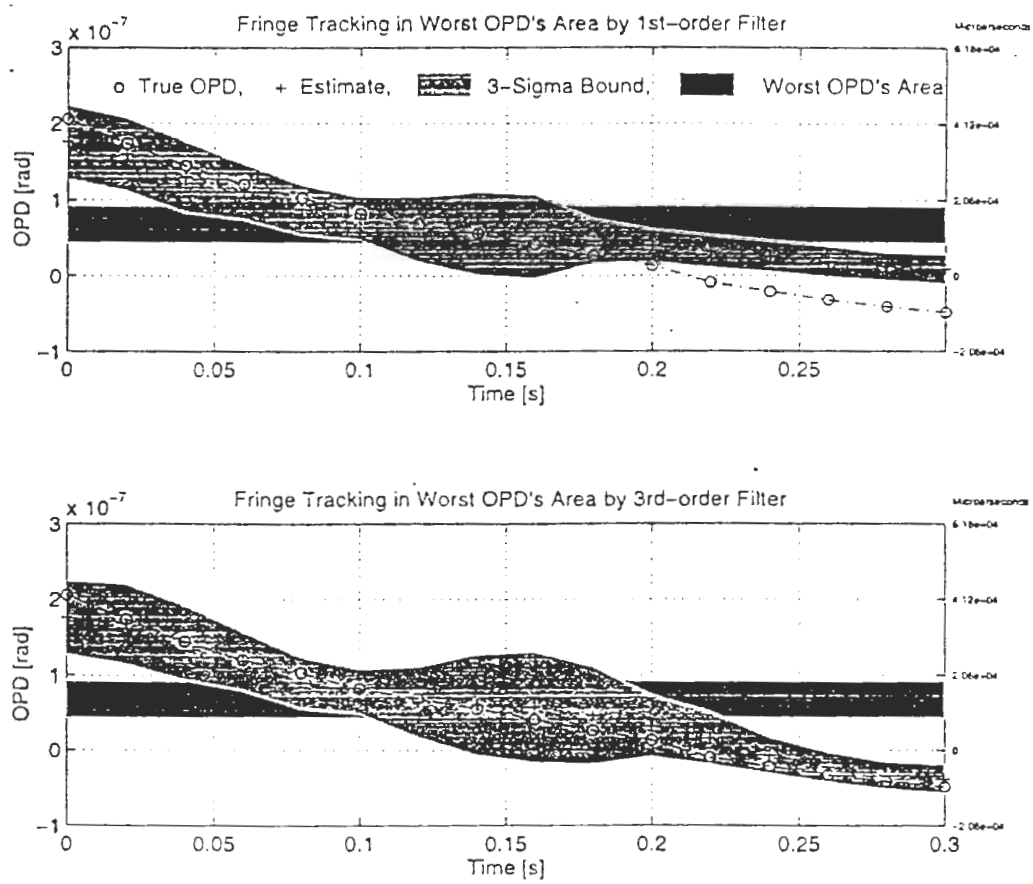

Figure 5 Operation of EKF and NEKF in Region of Low Sensitivities